Ouyang *et al.*
Protection and Control of Modern Power Systems (2023) 8:46
https://doi.org/10.1186/s41601-023-00323-9

Protection and Control of
Modern Power Systems

ORIGINAL RESEARCH

An improved prediction method of subsequent commutation failure of an LCC-HVDC considering sequential control response

Jinxin Ouyang[1*], Xinyu Pan[1], Junjun Ye[1], Chao Xiao[2], Yanbo Diao[3] and Qingwu Zhang[4]

Abstract

Subsequent commutation failure (SCF) can be easily generated during the first commutation failure (CF) recovery process in a line-commutated converter-based high voltage direct-current system. SCF poses a significant threat to the safe and stable operation of power systems, and accurate prediction of CF is thus important. However, SCF is affected by the operating characteristics of the main circuit and the coupling effects of sequential control response in the inverter station. These are difficult to predict accurately. In this paper, a new SCF prediction method considering the control response is proposed based on the physical principle of SCF. The time sequence and switching conditions of the controllers at different stages of the first CF recovery process are described, and the corresponding equations of commutation voltage affected by different controllers are derived. The calculation method of the SCF threshold voltage is proposed, and the prediction method is established. Simulations show that the proposed method can predict SCF accurately and provide useful tools to suppress SCF.

Keywords Line-commutated converter based high-voltage direct-current (LCC-HVDC), Subsequent commutation failure (SCF), Converter station, Prediction

1 Introduction

Line-commutated converter-based high-voltage direct current (LCC-HVDC) is widely used in long-distance transmission and asynchronous network connection because of its advantages of large transmission capacity and low power loss over long transmission distances [1, 2]. LCC-HVDC adopts thyristor valves without self-turning off capability, and thus, commutation failure (CF) can occur after faults at the receiving-end grid. CF can cause DC voltage drop, DC overcurrent, and significant transmission power reduction. Although LCC-HVDC can usually recover after the first CF, a subsequent commutation failure (SCF) could occur if the control of the converter is inappropriate or the fault lasts for a long time [3]. SCF can cause large power disruptions and even DC blocking. These bring serious challenges to the safe and stable operation of the power system.

CF prediction is beneficial because it enables taking measures in advance to prevent CF and ensure stable operation. The reason for CF is that the extinction angle (EA) is less than the minimum angle required for the valve to restore forward voltage blocking capability. Thus, EA is a direct criterion to estimate CF. However, the calculation of EA is updated after the complete voltage

*Correspondence:
Jinxin Ouyang
jinxinoy@163.com
[1] State Key Laboratory of Power Transmission Equipment and System Security and New Technology, School of Electrical Engineering, Chongqing University, Chongqing 400044, China
[2] Electric Power Research Institute of State Grid Henan Electric Power Company, Zhengzhou 450052, China
[3] Chongqing City Management College, Chongqing 401331, China
[4] NR Electric Co., Ltd, Nanjing 211100, China

waveform measurement, i.e., only at the point where the commutation voltage crosses zero. Therefore, the use of EA cannot predict CF correctly [4]. On the other hand, the transient process of DC current is closely related to the commutation process, and thus some researchers use the variation and mutation rate of DC current to predict CF [5, 6]. However, here accuracy depends on the fineness of the model, which is limited by parameters. The prediction in [7] based on a commutation area considers the influence of commutation voltage, DC current, and firing angle on the commutation process, but the commutation area is affected by many factors which reduce prediction accuracy [8].

Commutation voltage drop is usually the source of CF. Therefore, the commutation voltage can be used as an intuitive basis for CF prediction, while the voltage of the converter bus dropping to 90% is usually used to predict the first CF in practice [9]. However, this criterion lacks a theoretical basis and has limited effect. Some researchers calculate the CF threshold voltage based on the operating state and structure parameters of the power system with consideration of the transient change of DC current [10]. A CF prediction method combining the stability factor and interaction factor of voltage is proposed, which can quickly identify the risk area of CF [8, 11]. However, these studies aim at predicting the first CF after a grid fault, while the influencing factors on SCF are complex [12]. The first CF is mainly dominated by the response of the main circuit of the inverter station, while SCF is also affected by the sequential control response because SCF occurs when the control of the inverter station is fully functioning [13]. As the existing research on the first CF prediction ignores the control response, it cannot be directly used for SCF prediction.

Existing research on SCF focuses on the principal analysis and suppression measures, while there are few studies on SCF prediction. Researchers have used data-driven methods to search the variation law of electrical quantities to predict SCF. However, the training features are such that it is difficult to reflect the mapping relationship between data [14]. An SCF prediction method based on data-physical fusion is proposed in [15], but the error needs to be corrected continuously. Some propose a prediction method based on CF risk factor and phase detection [16], whereas others use the DC current [17], and commutation voltage [18] and voltage–time commutation area [19] after CF to predict the risk of SCF. However, the influence of the control response is ignored.

An improved prediction method of SCF considering the sequential control response of the inverter station is proposed in this paper. The equations of the commutation voltage are deduced by describing the time sequence and switching conditions of controllers at different stages of the first CF recovery process. A SCF threshold voltage considering the control response is modeled, one which considers the transient characteristics of DC current, firing angle, and EA. The threshold voltage depicts the coupling effect of sequential control response and commutation voltage during the first CF recovery process. Therefore, improved SCF prediction is realized by comparing the commutation voltage with the SCF threshold voltage.

The main contents of the paper are as follows: Sect. 2 analyzes the control response characteristics during the first CF recovery process, while Sect. 3 presents the prediction principle of SCF based on the commutation voltage. In Sect. 4, the commutation voltages at different stages of the first CF recovery process are derived, and a calculation method of the SCF threshold voltage is proposed. Section 5 verifies the proposed method using the CIGRE benchmark HVDC test system, and Sect. 6 draws conclusions.

2 Characteristics of subsequent commutation failure

A typical control system of the inverter station of an LCC-HVDC is shown in Fig. 1. It is generally equipped with a constant current controller (CCC), constant extinction angle controller (CEAC), voltage-dependent current order limiter (VDCOL), and current error controller (CEC) which is used to achieve smooth switching between the CEAC and the CCC. U_{d} and I_{d} are the DC voltage and DC current of the inverter station, respectively. γ is the EA and γ_0 is the initial EA. $I_{\mathrm{dr\text{-}ord}}$ is the DC current command value transferred from the inverter station to the rectifier station. This is the smaller value of the current references provided by the VDCOL and the master control. β is the firing angle, and β_{ccc} and β_{cea} are the firing angles provided by the CCC and CEAC, respectively. The larger value between

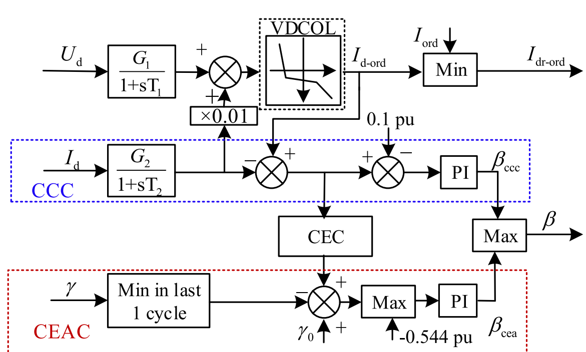

Fig. 1 Control system of the inverter station

the firing angles provided by the CCC and CEAC is typically selected as the command value of the firing angle.

CF is a dynamic event where a converter valve that is supposed to turn off but continues to conduct without transferring current to the next valve in the firing sequence [20]. The control of an inverter station causes the consumption of the reactive power to rise continuously and the commutation voltage to drop after the first CF, and this can cause SCF. The evolution process of SCF is shown in Fig. 2, where the process of the EA dropping to zero in a step is the first CF, while the process of the EA overshooting to dropping to 0 again is the first CF recovery process. The first CF recovery process can be divided into two stages according to the switching of CEAC and CCC. The inverter station is controlled by CCC in Stage 1 and by CEAC in Stage 2. The action of CEC in Stage 2 makes the EA drop sharply and leads to SCF.

Stage 1: the inverter station operates under CCC and VDCOL. The commutation is recovered in Stage 1, and the EA steps significantly higher than the normal EA at the moment of the first CF recovery because the continuous rise of the deviation of EA detected by the CEAC changes from a positive to a negative value, causing β_{cea} to drop rapidly. CEAC is switched to CCC when β_{cea} is less than β_{ccc} as shown by Switching 1 in Fig. 2. The measuring object of the control system switches from EA to DC current, and the DC current is controlled and restored gradually to the rated value by the VDCOL. During the DC current recovery process, the EA and DC voltage can be expressed as:

$$\begin{cases} \gamma = \arccos\left(\dfrac{\sqrt{2}NI_{\mathrm{d}}X_{\mathrm{r}}}{U_{\mathrm{L}}} + \cos\beta\right) \\ U_{\mathrm{d}} = \dfrac{3\sqrt{2}}{\pi}NU_{\mathrm{L}}\cos\gamma - \dfrac{3}{\pi}X_{\mathrm{r}}I_{\mathrm{d}} \end{cases} \tag{1}$$

where X_{r} is the converter reactance, U_{L} is the effective value of the line-to-line commutation voltage of the inverter station, and N is the ratio of converter transformer.

The following expression can be obtained from (1), as:

$$\frac{U_{\mathrm{dN}} + \frac{3}{\pi}X_{\mathrm{r}}I_{\mathrm{dN}}}{U_{\mathrm{d}} + \frac{3}{\pi}X_{\mathrm{r}}I_{\mathrm{d}}} = \frac{I_{\mathrm{dN}}}{I_{\mathrm{d}}}\frac{cos\gamma - \cos(\gamma+\mu)}{cos\gamma_0 - \cos(\gamma_0+\mu_0)}\frac{\cos\gamma_0}{\cos\gamma} \tag{2}$$

where U_{dN} and I_{dN} are the rated DC voltage and current of the inverter station, respectively. μ is the commutation overlap angle and μ_0 is its initial value.

The DC current is small during the first CF recovery process and the time to complete the current transfer is relatively short. Therefore, the commutation overlap angle in the fault should be small, but the difference is not significant, i.e., $\mu < \mu_0$.

There is usually a 0.1 pu current margin between the rectifier side and inverter side under the CCC. Therefore, the DC current can be expressed as [21]:

$$I_{\mathrm{d}} = \left(0.9\frac{U_{\mathrm{d}}}{U_{\mathrm{dN}}} + 0.09\right)I_{\mathrm{dN}} \tag{3}$$

Substituting (3) into (2) yields the following expression:

$$\frac{U_{\mathrm{d}}I_{\mathrm{dN}} + \frac{3}{\pi}X_{\mathrm{r}}I_{\mathrm{d}}I_{\mathrm{dN}} + (0.09U_{\mathrm{dN}} - 0.1U_{\mathrm{d}})I_{\mathrm{dN}}}{U_{\mathrm{d}}I_{\mathrm{dN}} + \frac{3}{\pi}X_{\mathrm{r}}I_{\mathrm{d}}I_{\mathrm{dN}}} = \frac{1 - \cos\mu + \tan\gamma\sin\mu}{1 - \cos\mu_0 + \tan\gamma_0\sin\mu_0} \tag{4}$$

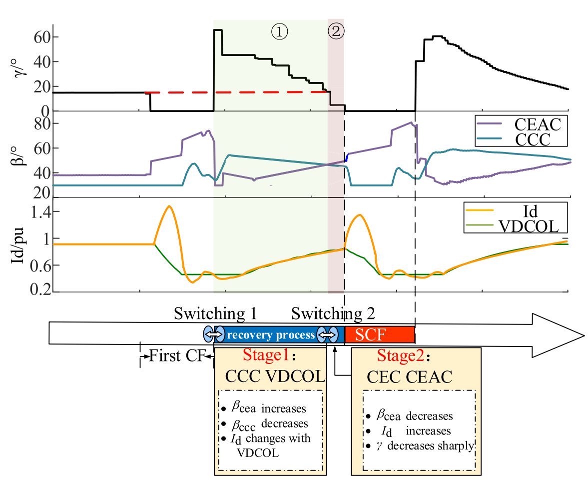

Fig. 2 Evolution process of commutation failure

VDCOL is triggered when $U_{\mathrm{d}} \le 0.9U_{\mathrm{dN}}$, and thus, $0.09U_{\mathrm{dN}} - 0.1U_{\mathrm{d}} \ge 0$. So the value of (4) is greater than or equal to 1, and the EA should satisfy:

$$\tan\gamma \ge \tan\gamma_0 \tag{5}$$

The EA is constantly greater than the rated value during Stage 1, according to (5). Therefore, SCF cannot occur during Stage 1.

Stage 2: the inverter station operates under the CEAC and CEC. The output of the CCC gradually decreases as the EA decreases and the DC current increases. The CCC switches to CEAC when the EA returns to the steady-state value [3], as shown by Switching 2 in Fig. 2. The CEC maintains the stability of the electrical quantities to guarantee the smoothness during the switching, and the control equation of the CEC can be written as:

$$\Delta\gamma_{\text{cec}} = \begin{cases} 0 & \Delta I_{\text{d}} > 0 \\ K_{\text{cec}}(I_{\text{d0}} - I_{\text{d}}) & 0 \le \Delta I_{\text{d}} \le \Delta I_{\text{H}} \\ \Delta\gamma_{\max} & \Delta I_{\text{d}} > \Delta I_{\text{H}} \end{cases} \tag{6}$$

where $\Delta\gamma_{\text{cec}}$ is the EA increment of the CEC, and $\Delta\gamma_{\max}$ is its upper limit. ΔI_{H} is the saturation value of the DC current deviation given as $\Delta I_{\text{H}}=0.1$. I_{d0} is the DC current command value of the rectifier station, $\Delta I_{\text{d}}=I_{\text{d0}}-I_{\text{d}}$, and K_{cec} is the slope of the CEC.

The CEC ensures a smooth transition of the DC current to the target current at the rectifier station and provides an EA increment to the CEAC. The DC current increases briefly under the CEC and $\Delta I_{\text{d}}>0.1$pu during Stage 2 [4]. The EA drops below the steady-state EA, and the output of the CEC decreases after Switching 2. The CEAC cannot respond effectively to the change in EA, and the firing angle still increases when the EA decreases. Meanwhile, the control switching causes the DC current to rise. The EA drops sharply under the CEC as it decreases with the increase of the DC current, and this may lead to SCF.

3 Prediction principle of subsequent commutation failure

Figure 3 shows the schematic diagram of SCF prediction. t_0, t_1, and t_2 are the start times of the first CF, first CF recovery, and SCF, respectively. The commutation voltage is affected by the EA, DC current, and firing angle during the first CF recovery process. Therefore, the commutation voltage depends on the fault severity and the control response, which corresponds to the EA under certain control parameters. SCF occurs in Stage 2 when the EA falls below the critical EA, and the commutation voltage is called the SCF threshold voltage when the EA is equal to the critical EA. It is noted that the commutation voltage should be less than the SCF threshold voltage, which is the necessary and sufficient condition of SCF.

The commutation voltage tends to decrease during the first CF recovery process, while it rises slightly because of the sudden increase of the EA after the converter restores commutation at t_1. The inverter station absorbs reactive power from the grid for a considerable period as the DC current is being restored. Thus, the commutation voltage drops again after the gird fault [18]. The commutation condition in Stage 2 cannot be satisfied because the commutation voltage decreases continuously if in Stage 1 it is lower than the SCF threshold voltage. At this point, SCF occurs in Stage 2. As the commutation voltage in Stage 2 is close to that at the end of Stage 1 because of the short duration of Stage 2, therefore SCF can be predicted in advance by comparing the commutation voltage in Stage 1 with the SCF threshold voltage.

The prediction method of SCF is shown in Fig. 4. As seen, the firing angle in Stage 1 and the SCF threshold voltage are calculated by the controller in advance. The commutation voltage and EA of the inverter station are measured in real-time after the first CF. The SCF prediction is initialized when the EA is detected to increase rapidly after a grid fault. The commutation voltage is collected and compared with the SCF threshold voltage in real-time, and the SCF in Stage 2 is detected in advance if the commutation voltage in Stage 1 is smaller than the SCF threshold voltage. The data acquisition, related calculation, and command determination modules are activated after a grid fault. The prediction can be executed in a fast DSP with an execution cycle of about 80 μs. Therefore, the control can be applied in real-time to avoid the occurrence of SCF or alleviate the influence of SCF based on the SCF prediction.

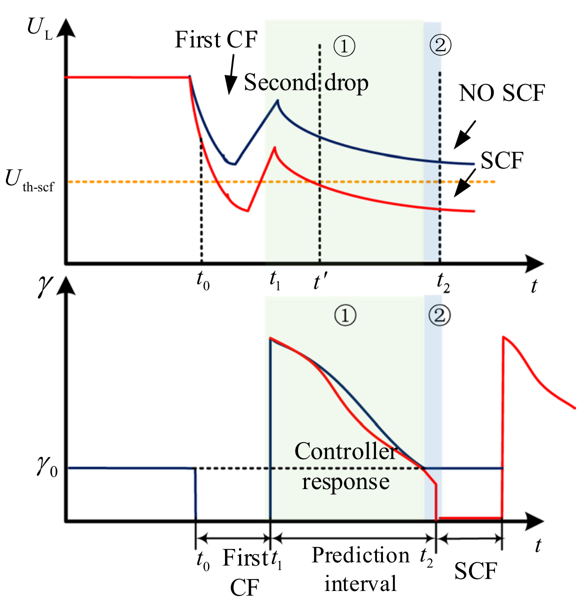

Fig. 3 Schematic diagram of SCF prediction

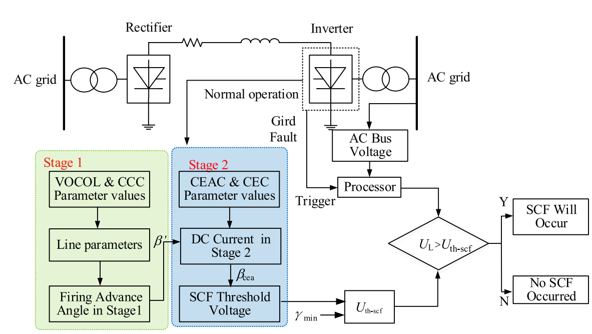

Fig. 4 Implementation of SCF prediction

4 Threshold voltage of subsequent commutation failure

4.1 Stage 1

The CCC adjusts the firing angle during Stage 1. It can be written as:

$$\beta_{ccc} = K_{p\text{-}ccc}\left\{\Delta I + \frac{1}{T_{i\text{-}ccc}}\int \Delta I dt\right\} \tag{7}$$

where $K_{p\text{-}ccc}$ and $T_{i\text{-}ccc}$ are the proportional coefficient and integral time constant of the CCC, respectively. ΔI is the current deviation and $\Delta I = I_{dro} - i_d - 0.1$, I_{dro} is the reference value of the rectifier DC current, and i_d is the measured inverter DC current.

The integral function is reserved in (7) and the derivation process, so the nonlinear characteristics caused by the integral link are considered.

The DC current follows the reference value of the rectifier side with a small difference, and thus ΔI can be considered to be constant.

The derivation (7) of can be obtained as:

$$\frac{d\beta_{ccc}}{dt} = \frac{K_p}{T_i}(I_{dro} - i_d - 0.1) \tag{8}$$

Equation (8) can be transformed as:

$$\frac{d\beta_{ccc}}{dt} = \frac{d\beta_{ccc}}{di_d}\cdot\frac{di_d}{dt} = \frac{d\beta_{ccc}}{di_d}\cdot k_i \tag{9}$$

Because of the rapid transient response, Eq. (9) can be linearized based on the minimum deviation method as [22]:

$$k_i = \frac{U_{dor}}{R_{cr} + R_L - R_{ci}} \tag{10}$$

where U_{dor} indicates the ideal no-load DC voltage of the rectifier station, R_L is the DC resistance, while R_{cr} and R_{ci} are the equivalent commutation resistances of the rectifier and inverter, respectively.

The dynamic equation of the firing angle can be obtained from (9) as:

$$\frac{d\beta_{ccc}}{di_d} = \frac{K_{p\text{-}ccc}}{k_i T_{i\text{-}ccc}}(I_{dro} - i_d - 0.1) \tag{11}$$

According to (11), the firing angle under the CCC can be calculated by:

$$\beta_{ccc} = -\frac{K_{p\text{-}ccc}}{2k_i T_{i\text{-}ccc}} i_d^2 + \frac{(I_{dro} - 0.1)K_{p\text{-}ccc}}{k_i T_{i\text{-}ccc}} i_d + C_1 \tag{12}$$

and

$$i_d = \frac{U_{dor}\cos\alpha - U_{doi}\cos\gamma}{R_{cr} + R_L - R_{ci}} \tag{13}$$

where U_{doi} is the ideal no-load DC voltage of the inverter station, α is the firing angle of the rectifier station, and C_1 is the integral constant.

The current command provided by the VDCOL gradually rises because of the recovery of the DC voltage during Stage 1. When the DC current closes to the command value, the CCC adjustment of the rectifier station is largely over, and the firing angle of the rectifier station closes to 45° [22]. The CCC plays a leading role in the inverter station, and the DC current can be written as:

$$I_d = kU_d + b \tag{14}$$

From the state equations of the inverter station, the relationship between the DC voltage and DC current can be written as:

$$U_d = \frac{3\sqrt{2}}{\pi}NU_L\cos\gamma - \frac{3}{\pi}X_r I_d \tag{15}$$

Substituting (14) into (15), the DC voltage considering the effect of the VDCOL can be expressed as:

$$U_d = \frac{3\sqrt{2}}{\pi}NU_L\cos\gamma - \frac{3}{\pi}X_r(kU_d + b) \tag{16}$$

The DC voltage can be written as:

$$U_d = \frac{3\sqrt{2}}{2\pi}NU_L(\cos\gamma + \cos\beta_{ccc}) \tag{17}$$

From (16) and (17), the commutation voltage considering the effect of the CCC and VDCOL can be obtained by:

$$U_{L1} = \frac{\frac{3}{\pi}X_r b}{\frac{3\sqrt{2}}{\pi}N\cos\gamma - \frac{3\sqrt{2}}{2\pi}N\left(1 + \frac{3}{\pi}kX_r\right)(\cos\gamma + \cos\beta_{ccc})} \tag{18}$$

According to the parameters of LCC-HVDC [23], the sensitivity of commutation voltage with change of EA should meet:

$$\frac{\partial U_{L1}}{\partial\gamma} > 0 \tag{19}$$

Equation (19) reflects the influence of the variation of EA on the commutation voltage under the effects of the CCC and VDCOL in Stage 1. The commutation voltage decreases with the reduction of EA during the first CF recovery process according to (19).

4.2 Stage 2

The inverter station is switched to the CEAC at the moment that the EA reaches the rated EA when the firing angle provided by the CCC is less than that by the CEAC. The target of the CEAC is to keep the firing angle of the inverter station at rated value [3], and the control equation is given by:

$$\beta_{\text{cea}} = K_{\text{p-cea}}\left\{[\gamma_0 - \gamma + \Delta\gamma_{\text{cec}}] + \frac{1}{T_{\text{i-cea}}}\int[\gamma_0 - \gamma + \Delta\gamma_{\text{cec}}]dt\right\} \tag{20}$$

where $K_{\text{p-cea}}$ and $T_{\text{i-cea}}$ are the proportional coefficient and integral time constant of the CEAC, respectively.

The EA of the inverter station is measured when the CEAC works. The control system is usually updated every 1.67 ms and the integral time constant of the CEAC is usually 54.4 ms. The interval between the action of the CEAC and the occurrence of SCF is generally 4–8 ms [12]. Therefore, the output of the integral controller of the CEAC can be approximated to 0 before SCF occurs [3]. The CEC plays the leading role in the meantime. At the moment of Switching 2, $\Delta\gamma_{\text{cec}}$ is at its maximum and β_{cea} can be expressed as:

$$\beta_{\text{cea}} = \beta' + K_{\text{p-cea}}(\gamma_0 - \gamma + \Delta\gamma_{\text{cec}}) \tag{21}$$

where β' is determined by β_{ccc} when $\gamma = \gamma_0$ in (12).

From (6), the EA under the effect of CEC can be expressed as:

$$\gamma = \gamma_0 + K_{\Delta i}(I_{\text{d0}} - I_{\text{d}})/I_{\text{d0}} \tag{22}$$

where I_{d0} is the current setting value of the rectifier station, and $K_{\Delta i}$ is the proportional coefficient of the CEC.

Under the CEC, the DC current can be expressed as:

$$I_{\text{d}} = I_{\text{d0}} + (\gamma_0 - \gamma)\frac{I_{\text{d0}}}{K_{\Delta i}} \tag{23}$$

By substituting (23) into (15), the DC voltage can be obtained as:

$$U_{\text{d}} = \frac{3\sqrt{2}}{\pi}NU_{\text{L}}\cos\gamma - \frac{3}{\pi}X_{\text{r}}\left[I_{\text{d0}} + (\gamma_0 - \gamma)\frac{I_{\text{d0}}}{K_{\Delta i}}\right] \tag{24}$$

Under the CEAC, the DC voltage can be obtained by:

$$U_{\text{d}} = \frac{3\sqrt{2}}{2\pi}NU_{\text{L}}\left(\cos\gamma + \cos\left[\beta_0 + K_{\text{p-cea}}(\gamma_0 - \gamma + \Delta\gamma_{\text{cec}})\right]\right) \tag{25}$$

Combining (24) and (25), the commutation voltage considering the effects of the CEAC and CEC can be expressed as:

$$U_{\text{L2}} = \frac{\frac{3}{\pi}X_{\text{r}}\left[I_{\text{d0}} + (\gamma_0 - \gamma)\frac{I_{\text{d0}}}{K_{\Delta i}}\right]}{\frac{3\sqrt{2}}{\pi}N\cos\gamma - \frac{3\sqrt{2}}{2\pi}N(\cos\gamma + \cos\beta_{\text{cea}})} \tag{26}$$

where

$$\beta_{\text{cea}} = \beta' + K_{\text{p}}[\gamma_0 - \gamma + \Delta\gamma_{\text{cec}}] \tag{27}$$

The sensitivity of U_{L2} with the change of EA can be calculated according to (26) as:

$$\frac{\partial U_{\text{L2}}}{\partial\gamma} > 0 \tag{28}$$

According to (28), the commutation voltage decreases with the reduction of EA in Stage 2. By substituting the critical EA, the SCF threshold voltage can be obtained as:

$$U_{\text{th-SCF}} = \frac{\frac{3}{\pi}X_{\text{r}}\left[I_{\text{d0}} + (\gamma_0 - \gamma_{\min})\frac{I_{\text{d0}}}{K_{\Delta i}}\right]}{\frac{3\sqrt{2}}{\pi}N\cos\gamma_{\min} - \frac{3\sqrt{2}}{2\pi}N(\cos\gamma_{\min} + \cos\beta_{\text{cea}})} \tag{29}$$

β_{ccc} under the effects of the VDCOL and CCC can be calculated by (12) according to the circuit and controller parameters of the LCC-HVDC. Therefore, β' at Switching 2 can also be calculated by (12). The SCF threshold voltage can be obtained by (29) through β_{cea} and I_{d} under the effects of the CEAC and CEC from (21) and (23). Compared with the CF threshold voltage in [24, 25], the SCF threshold voltage contains the control response of the VDCOL and CCC in Stage 1, and the CEAC and CEC in Stage 2, while also considering the effect of DC current rise and the change of firing angle on the EA.

5 Case study

The CIGRE benchmark HVDC test system [26] is used to verify the theoretical analysis using PSCAD/EMTDC. The operational parameters are as follows: $U_{\text{dr0}} = 219.16$ kV, $i_0 = 277.58$ kV, $R_{\text{d}} = 5\ \Omega$, $R_{\text{cr}} = 12.96\ \Omega$, $R_{\text{ci}} = 12.72$*2 Ω, $X_{\text{c}} = 13.32\ \Omega$, $I_{\text{d}} = 2$ kA, $N = 211.42/230$ kV, $K_{\Delta i} = 0.15$. The proportional coefficient of the CCC is 0.7506, and the integral time constant is 0.0544. In the VDCOL, the upper and lower limits of DC current are 1.0 pu and 0.55 pu, respectively, while the upper and lower thresholds of the DC voltage are 0.9 pu and 0.4 pu, respectively. the voltage of the converter bus is 230 kV, the DC current is 2 kA, the EA is 15.2° and the firing angle is 38.3° at the inverter station under normal operation.

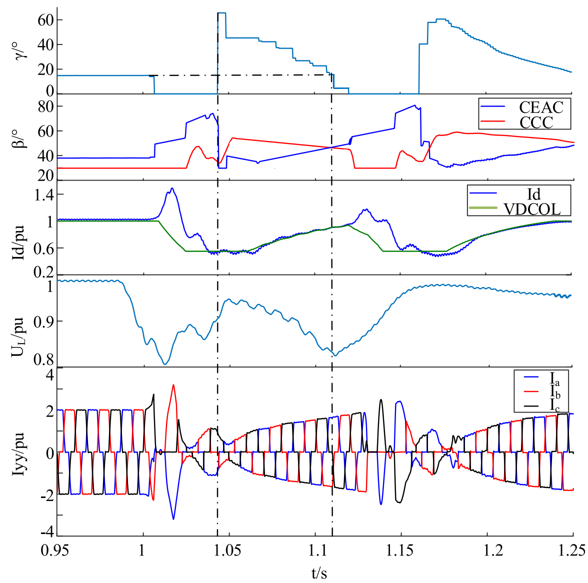

Fig. 5 Electrical quantities under single-phase fault

5.1 Recovery characteristics

A single-phase fault is set at the inverter bus with the fault inductance of 0.6 H. The fault occurs at 1 s and has a duration of 0.1 s. As shown in Fig. 5, the EA decreases and the valve current reduces to 0 during the first CF. The firing angle determined by the CEAC gradually increases after the fault. Stage 1 begins when the commutation restores, and the control of the inverter station is switched from the CEAC to CCC at 1.042 s. The DC current changes with the command value of the VDCOL, and the commutation voltage drops again. During Stage 1, the EA of the inverter station is always above the critical EA, and there is no SCF. The command value determined by the CEAC then gradually increases during the first CF recovery process. The EA is restored to the rated EA, and the control is switched back to the CEAC when the EA is 15°. During Stage 2, the EA drops below the steady-state EA and continuously decreases to below the critical EA under the effect of the CEC. Consequently, SCF occurs at 1.125 s. The evolution process of the CF obtained by the simulation is consistent with the previous theoretical analysis.

5.2 Subsequent commutation failure prediction

To verify the effectiveness of the proposed SCF prediction, the following three methods are compared.

Method 1: the threshold voltage considering DC current rise and AC voltage drop in [24] is adopted, and is calculated by:

$$U_{\text{th1}} = \frac{\sqrt{2}X_r U_{\text{dr0}} \cos\alpha}{\frac{6X_r}{\pi} + R_{\text{cr}} + R_d - R_{\text{ci}}} \cdot \frac{1}{\cos\gamma_{\min} - \frac{R_{\text{cr}}+R_d-R_{\text{ci}}}{\frac{6X_r}{\pi}+R_{\text{cr}}+R_d-R_{\text{ci}}}} \tag{30}$$

where $\gamma_{\min}$ is the critical extinction angle.

Method 2: the threshold voltage considering the change of DC current in [25] is adopted, and is calculated by:

$$U_{\text{th2}} = U_{\text{LN}}\sqrt{\frac{\cos^2\gamma_0 - \cos^2\beta}{\cos^2\gamma_{\min} - \cos^2\beta}} \tag{31}$$

where U_{LN} is the rated effective value of the line-to-line commutation voltage of the inverter station.

Method 3: the SCF threshold voltage proposed in this study is adopted, and is calculated by (29).

The comparison of the relationships between the commutation voltage and EA for Methods 1, 2 and 3 is shown in Fig. 6, in which the slopes of the curves reflect the degree of change in EA caused by commutation voltage drop. The threshold voltages of Methods 1 and 2 are 223.6 kV and 216.2 kV, respectively, when $\gamma = \gamma_{\min}$ as indicated in the red dashed line in Fig. 6. In comparison, the SCF threshold voltage of Method 3 is 202.1 kV. The firing angles are assumed not to change abruptly in Methods 1 and 2, while the control responses during the first CF recovery process were also not considered by Methods 1 and 2. The curves show that the threshold voltages calculated by the three methods are clearly different, indicating that the 'negligence' and simplification of Methods 1 and 2 have significant influence on the calculated commutation voltages.

The impedance of high voltage lines is mainly inductive, and the resistance component in the transition impedance is generally much smaller than the line inductance in the HVDC system fault analysis. Thus, the grounding impedance at the converter bus can be set to inductive to simulate the grounding fault on the remote lines. Single-phase, two-phase and three-phase faults are set at the converter bus of the inverter station with the fault inductances varying from 0.35 H to 0.80 H. With the decrease in fault inductances, the equivalent fault location is closer to the AC bus, i.e., the fault is more severe. From Fig. 4, β' calculated by (12) is 37.9° when $\gamma = \gamma_0$. Thus, the SCF threshold voltage of Method 3 calculated by (29) is 0.879 pu, whereas the SCF threshold voltages of Methods 1 and 2 calculated by (30) and (31) are 0.94 pu and 0.97 pu, respectively. The EA and commutation voltage of the inverter station under single-phase, two-phase and three-phase faults are obtained by simulation as shown in Fig. 7, 8 and 9, respectively.

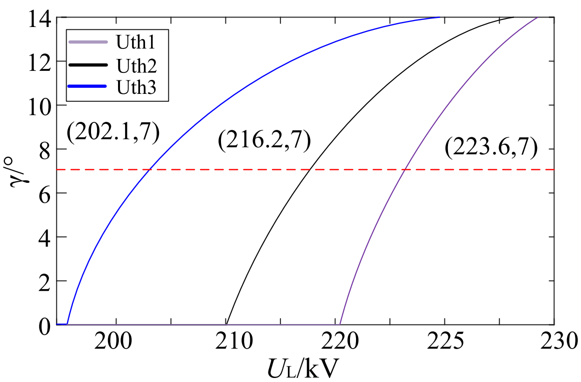

Fig. 6 Relationship between commutation voltage and EA

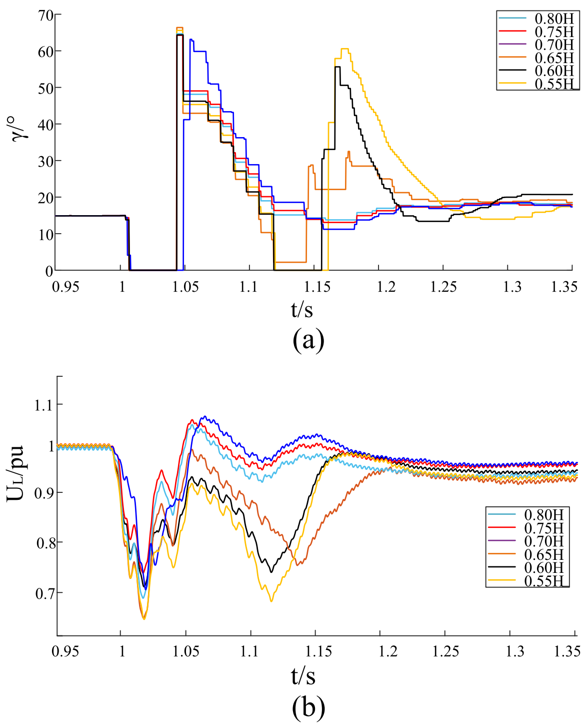

Fig. 7 Electrical quantities under single-phase fault with different fault inductances. **a** Extinction angle **b** commutation voltage

As shown in Fig. 7, the minimum commutation voltages during the first CF recovery process are 0.935 pu, 0.922 pu and 0.91 pu when the fault inductances are 0.7 H, 0.75 H and 0.8 H under the single-phase fault, respectively. As the commutation voltages are higher than the SCF threshold voltage of Method 3, it predicts that SCF will not occur, which matches the situation shown in Fig. 7a. However, the minimum commutation voltage is lower than the threshold voltages of Methods 1 and 2, and thus, wrong prediction would be provided by

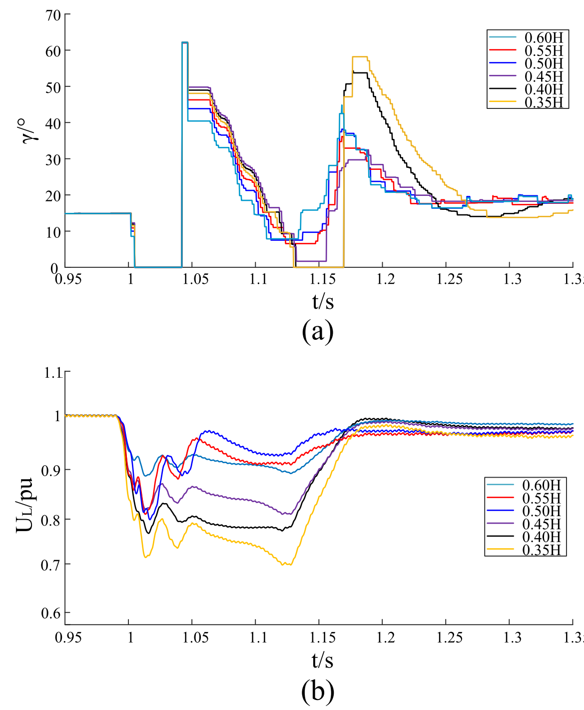

Fig. 8 Electrical quantities under three-phase fault with different fault inductances. **a** Extinction angle **b** commutation voltage

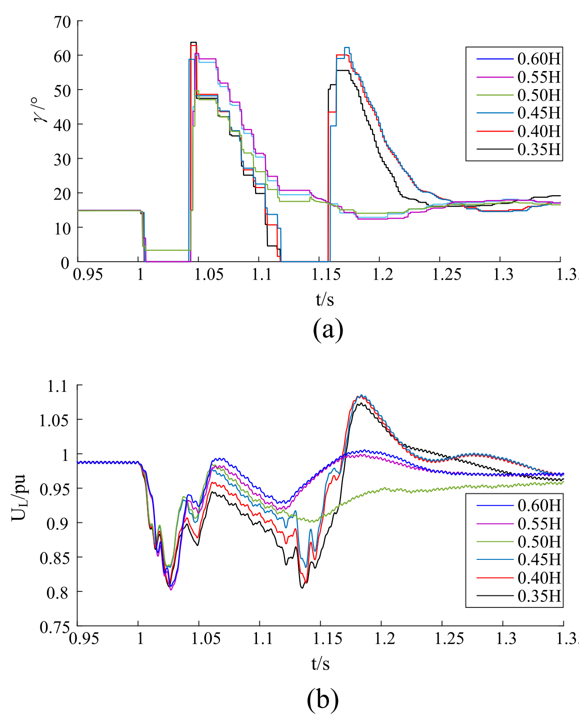

Fig. 9 Electrical quantities under two-phase fault with different fault inductances. **a** Extinction angle **b** commutation voltage

Methods 1 and 2. In Fig. 7b, the commutation voltages drop to the SCF threshold voltage obtained by Method 3 at 1.052 s, 1.056 s and 1.058 s, and decrease continuously under the single-phase fault when the fault inductances are from 0.55 H to 0.65 H. According to Fig. 7a, SCF occurs at 1.11 s, 1.12 s, and 1.13 s, respectively. Thus, Method 3 has correctly predicted SCF for different fault inductances.

As shown in Fig. 8, the minimum commutation voltages are 0.921 pu, 0.915 pu, and 0.902 pu when the fault inductances are from 0.5 H to 0.6 H under the three-phase fault, respectively. The commutation voltages are higher than the SCF threshold voltage obtained by Method 3, which correctly predicts that SCF will not occur. In contrast, Methods 1 and 2 predict the occurrence of SCF because the commutation voltages are lower than the threshold voltage, resulting in misjudgment. According to Fig. 8b, the commutation voltages drop to the threshold voltage of Method 3 at the beginning of recovery when the fault inductances are from 0.35 H to 0.45 H, and consequently, Method 3 is able to correctly predict SCF, as shown in Fig. 8b.

As shown in Fig. 9, the minimum commutation voltages are 0.901 pu, 0.918 pu, and 0.928 pu when the fault inductances are from 0.5 to 0.6 H under the two-phase fault, respectively. The commutation voltages are higher than the SCF threshold voltage obtained by Method 3, which correctly predicts that SCF will not occur. However, Methods 1 and 2 predict the occurrence of SCF because the commutation voltages drop to the threshold voltage, resulting in misjudgment. The minimum commutation voltages are 0.801 pu, 0.812 pu, and 0.835 pu when the fault inductances are from 0.35 H to 0.45 H, respectively, which are all less than 0.879 pu. Consequently, Method 3 correctly predicts that SCF will occur, which is in line with the actual situation.

Fault severity can be characterized by the commutation voltage, fault inductance, and rated power [27]. The fault time changes from 1 s to 1.024 s, and the fault type includes single-phase, two-phase and three-phase faults. The fault duration is 0.15 s. The results of SCF prediction obtained by the proposed method are shown in Fig. 10 when the fault severity changes from 0 to 70%. The abscissa is the fault time, and the ordinate is the fault severity, whereas the number is the minimum commutation voltage during the first CF recovery process. The green color indicates that only the first CF occurs, and the yellow and purple colors indicate that SCF occurs.

The commutation voltage is greater than the SCF threshold voltage, and SCF does not occur when the fault severity is from 0 to 40%, as shown in Fig. 10. However, SCF occurs when the fault severity is from 40 to 70%. The commutation voltage in the yellow grid is less than

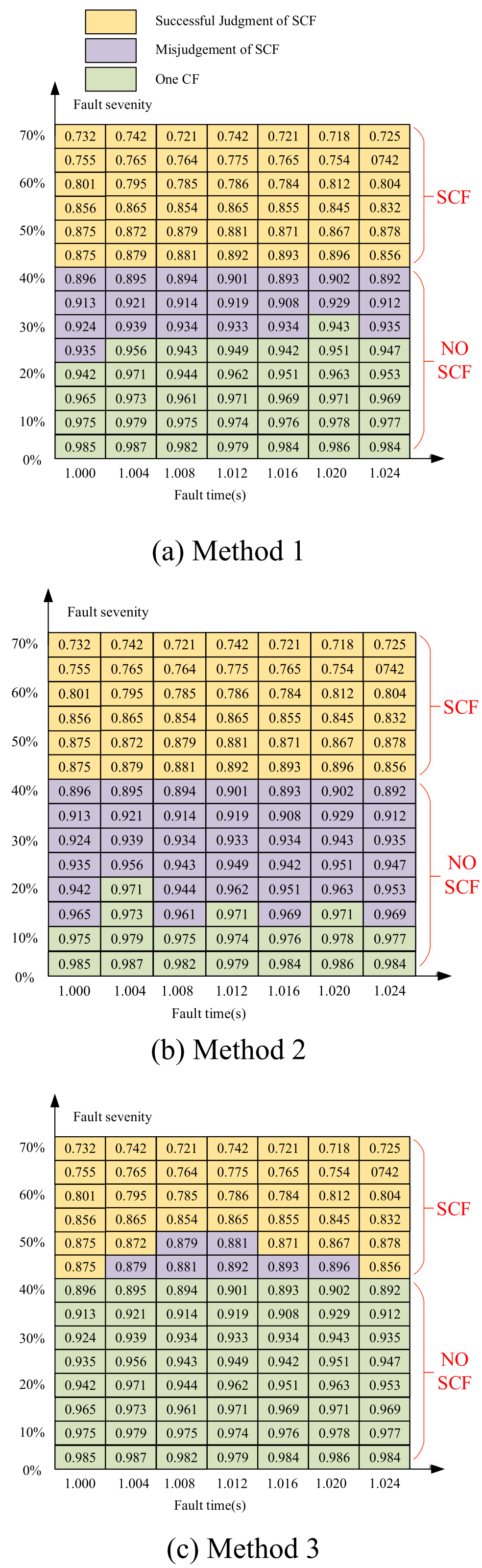

Fig.10 Accuracy of the SCF prediction

Table1 Advance Time and Result for SCF Prediction

Fault severity (/%)	Method 1		Method 2		Method 3		Occurrence time of SCF (/s)
	Prediction result (F/T)	Advance time (/ms)	Prediction result (F/T)	Advance time (/ms)	Prediction result (F/T)	Advance time (/ms)	
15	T	–	T	–	T	–	–
25	T	–	F	–	T	–	–
35	F	–	F	–	T	–	–
45	T	69.3	T	80.3	T	60.3	1.1213
55	T	73.5	T	81.5	T	65.5	1.1215
65	T	79.7	T	84.7	T	67.7	1.1217
75	T	82.1	T	87.1	T	72.1	1.1211

the SCF threshold voltage, thus indicating that the proposed method has predicted SCF accurately. The accuracy of the proposed method in predicting SCF is 92.8% in 98 fault tests. In contrast, Methods 1 and 2 have cases of misjudging one CF as SCF, and the accuracies are only 78.6% and 61.2%, respectively.

Methods 1 and 2 do not consider the influence of the controller response, whereas the threshold voltage of Method 3 takes into account the controller response and accounts for the transient change characteristics of DC current, α, β, and γ. Thus, Method 3 can predict the occurrence of SCF more accurately. The shortcoming of the proposed Method 3 is that it ignores the effect of the rising current on the EA during the CEC action period, which leads to the fall of the EA. Because the response of CEC has a delay, the EA may fall sharply in Stage 2, and thus, Method 3 may misjudge.

Table 1 shows the prediction results and advance time of SCF for the three methods with different severities. "T" indicates correct prediction, and "F" indicates wrong prediction. When the fault severity is 15–35%, SCF does not occur, so the occurrence time and advance time are blank, but Methods 1 and 2 judge that SCF will occur. When the fault severity is from 45 to 75%, the threshold voltages of Methods 1, 2, and 3 are 0.94 pu, 0.97 pu, and 0.879 pu, respectively. The threshold voltages of Methods 1 and 2 are larger than that of Method 3, and there is a delay in the voltage drop. Methods 1 and 2 can get the prediction results earlier in the same correct prediction, but the difference in advance time compared with Method 3 is small. The accuracies of the three methods with different severities are also shown in Table 1. As seen, the system does not have SCF when the fault severity is low, but Methods 1 and 2 may still misjudge SCF occurrence. In contrast, the prediction of Method 3 is correct.

With the increase in fault severity, the commutation voltage drops more significantly, i.e., the threshold voltage time is earlier. The longest advance time is 72.1 ms, the shortest is 60.3 ms, with the average being 66 ms. The SCF prediction provides sufficient time for adjustment to mitigate CF.

6 Conclusion

SCF can be easily triggered by the improper interaction of controllers during the first CF recovery process of LCC-HVDC. Prediction of SCF provides a powerful tool for the control and protection of LCC-HVDC and the power grid. However, the influencing factors on SCF are complex. In particular the effects of the sequential control response cannot be easily quantized. Therefore, the time sequence and switching conditions of the controllers of inverter station at different stages of the first CF recovery process are analyzed in this paper. A new SCF threshold voltage considering the control response is deduced, and an improved method for predicting SCF is proposed. The method can effectively predict SCF and has the advantages of clear physical concept and high accuracy. This method can also provide a reference for research on and implementation of CF suppression, and control and protection of the power grid. The prediction of SCF helps the development of control strategies in advance, and this enables HVDC to satisfy commutation requirements.

Acknowledgements
Not applicable.

Author contributions
JO: Conceptualization, Methodology, Software, Investigation, Writing—Original Draft, Supervision. XP: Validation, Formal analysis, Visualization, Software, Writing—Original Draft. JY: Investigation, Writing: Review & Editing. CX: Writing: Review & Editing. YD: Writing: Review & Editing. QZ: Writing: Review & Editing.

Funding
This work was supported in part by the National Natural Science Foundation of China under Grant (51877018).

Availability of data and materials
Not applicable.

Declarations

Competing interests
The authors declare that they have no known competing financial interests or personal relationships that could have appeared to influence the work reported in this paper.

Received: 8 December 2022 Accepted: 6 September 2023
Published online: 20 September 2023

References

1. Zhao, Y., Ma, J., Jiang, T., et al. (2021). Commutation failure prediction method based on characteristic of accumulated energy in inverter. *International Journal of Electrical Power and Energy Systems, 133*, 141–149.

2. Mohan, M. (2021). A comprehensive review of DC fault protection methods in HVDC transmission systems. *Protection and Control of Modern Power Systems, 6*(1), 1–20.
3. Liu, L., Lin, S., Liu, J., et al. (2020). Analysis and prevention of subsequent commutation failures caused by improper inverter control interactions in HVDC systems. *IEEE Transactions on Power Delivery, 35*(6), 2841–2852.
4. Rahimi, E., Gole, A. M., Davies, J. B., Fernando, I. T., & Kent, K. L. (2011). Commutation failure analysis in multi-infeed HVDC systems. *IEEE Transactions on Power Delivery, 26*(1), 378–384.
5. Shen, H., Huang, S., Fei, B., et al. (2016). A new method to detect commutation failure based on mathematical morphology. *Transactions of China Electrotechnical Society., 31*(4), 170–177.
6. Li, G., Wang, T., Xin, Y., et al. (2022). A rapid identification method for commutation failure risk area in multi-infeed high voltage direct current receiving-end power grid. *Proceedings of the CSEE, 42*(1), 140–153.
7. Zhu, R., Zhou, X., Xia, H., Hong, L., et al. (2022). Commutation failure mitigation method based on imaginary commutation process. *Journal of Modern Power Systems and Clean Energy, 46*(3), 156–163.
8. Xiao, H., Li, Y., & Duan, X. (2021). Enhanced commutation failure predictive detection method and control strategy in multi-infeed LCC-HVDC systems considering voltage harmonics. *IEEE Transactions on Power Systems, 36*(1), 81–96.
9. Zhao, L., Zhao, Y., Hong, C., et al. (2014). Analysis on commutation failure of the CSG's HVDC systems based on actual waves. *Southern Power System Technology, 8*(4), 42–46.
10. Lin, L., Zhang, Y., Zhong, Q., et al. (2007). Fault diagnosis of commutation failures in the HVDC system based on a method of wavelet energy statistics. *Automation of Electric Power Systems, 31*(23), 61–64.
11. Xiao, H., Duan, X., Zhang, Y., Lan, T., & Li, Y. (2022). Analytically quantifying the impact of strength on commutation failure in hybrid multi-infeed HVDC systems. *IEEE Transactions on Power Electronics, 37*(5), 4962–4967.
12. Ouyang, J., Zhang, Z., Li, M., Pang, M., et al. (2021). A predictive method of LCC-HVDC continuous commutation failure based on threshold commutation voltage under grid fault. *IEEE Transactions on Power Systems, 36*(1), 118–126.
13. Ouyang, J., Ye, J., Zhang, Z., et al. (2021). Prevention control method of subsequent commutation failure for LCC-HVDC under grid fault. *International Transactions on Electrical Energy System, 31*(9), 12–25.
14. Wei, Z., Yuan, Y., Lei, X., et al. (2014). Direct-current predictive control strategy for inhibiting commutation failure in HVDC converter. *IEEE Transactions on Power Systems, 29*(5), 2409–2417.
15. Wang, Q., Zhang, C., Lu, Y., et al. (2019). Data inheritance–based updating method and its application in transient frequency prediction for a power system. *International Transactions on Electrical Energy Systems, 29*(6), 12–25.
16. Cai, W., Yang, G., Du, D., et al. (2019). Prediction and identification method for commutation failure considering multi-factor influence. *Power System Technology, 43*(10), 3477–3487.
17. Zhou, B., Li, F., Song, X., et al. (2019). Commutation failure prediction and control system optimization based on DC current variation. *Power System Technology, 43*(10), 3497–3504.
18. Tang, Y., Zheng, C., Lou, B., et al. (2019). Research on DC power control strategy for mitigating continuous commutation failure. *Power System Technology, 43*(10), 3514–3522.
19. Zhu, R., Zhou, X., Xia, H., et al. (2022). A commutation failure prediction and mitigation method. *Journal of Modern Power Systems and Clean Energy, 10*(3), 779–787.
20. Zhen, L., Gao, H., Luo, S., et al. (2020). A fast boundary protection for an AC transmission line connected to an LCC-HVDC inverter station. *Protection and Control of Modern Power Systems., 5*(1), 1–12.
21. Zhu, L., Niu, C., Wang, Z., et al. (2021). An extinction angle dynamic compensation control method for suppressing continuous commutation failure. *Proceedings of the CSEE, 41*(22), 7621–7631.
22. Wang, T., Sun, Y., Pei, L., Wang, J., & Wang, Z. (2022). Analysis of DC current transient characteristics of LCC-HVDC considering control system and approximate analytical method of AC short-circuit current. In *Proceedings of the CSEE*, 2022.
23. Faruque, M. O., Zhang, Y., & Dinavahi, V. (2006). Detailed modeling of CIGRE HVDC benchmark system using PSCAD/EMTDC and PSB/SIMULINK. *IEEE Transactions on Power Delivery, 21*(1), 378–387.
24. Wang, F., Liu, T., Li, X., et al. (2016). Commutation failure analysis considering DC current rise and AC voltage drop speed. *Automation of Electric Power Systems, 40*(22), 111–117.
25. Xu, J., Tan, H., Sun, H., et al. (2015). Research on method to analyze commutation failure in HVDC power transmission system considering the impact of DC current variation and occurrence moment of AC fault. *Power System Technology., 39*(5), 1261–1267.
26. Zhou, H., Yao, W., Ai, X., et al. (2022). Coordinated power control of electrochemical energy storage for mitigating subsequent commutation failures of HVDC. *International Journal of Electrical Power and Energy Systems, 134*, 10745.
27. Guo, C., Liu, Y., Zhao, C., et al. (2015). Power component fault detection method and improved current order limiter control for commutation failure mitigation in HVDC. *IEEE Transactions on Power Delivery, 30*(3), 1585–1593.

Jinxin Ouyang male, currently an associate professor at School of Electrical Engineering, Chongqing University, China. His research interests include analysis, protection and control of renewable energy integrated power system, active distribution network and application of power electronic technology in power system.

Xinyu Pan female, currently pursuing the M.Sc. degree at the School of Electrical Engineering, Chongqing University, China. Her research interests include protection and control of renewable energy integrated power system.

Junjun Ye male, currently pursuing the M.Sc. degree at the School of Electrical Engineering, Chongqing University, China. His research interests include protection and control of renewable energy integrated power system.

Chao Xiao male, currently an engineer at the Electric Power Research Institute of State Grid Henan Electric Power Company, China.

Yanbo Diao female, currently a professor at Chongqing City Management College, Chongqing, China. Her research interests include system simulation and big data analysis.

Qingwu Zhang male, currently an engineer at NR Electric Co., Ltd, China.